8. The Solar-Wind Composition Experiment

J. Geiss,[a†] *P. Eberhardt,*[a] *P. Signer,*[b] *F. Buehler,*[a] *and J. Meister* [a]

The abundances of H^+ and He^{2+} ions in the solar wind have been monitored for several years (refs. 8–1 to 8–3). The He/H ratio is highly variable with time and ranges from less than 0.01 to 0.25 (ref. 8–1) with an average of about 0.04 (refs. 8–1 and 8–4 to 8–6). Oxygen ions have been measured during periods of low ion temperature by means of unmanned satellites and space probes; under very favorable conditions, even ^3He has been detected (ref. 8–7). The Apollo program has made it possible to introduce a new approach to the measurement of solar-wind ion composition. Targets can be exposed to the solar wind outside the magnetosphere of the Earth. In this way, solar-wind ions can be collected for laboratory analysis after return of the target. An experiment of this kind, the solar-wind composition experiment (refs. 8–8 and 8–9), was flown for the first time on the Apollo 11 mission. The experiment has yielded absolute solar-wind fluxes of ^4He, ^3He, ^{20}Ne, and ^{22}Ne averaged over a 77-min exposure period.

Prior to the first manned landing on the Moon, Explorer 35 plasma and magnetic field measurements had established that, to a good approximation, the Moon behaves like a passive obstacle to the solar wind, and no evidence for a bow shock had been observed (refs. 8–10 and 8–11). Thus, during the normal lunar day, the solar-wind particles were expected to strike the lunar surface with essentially unchanged energy. This was substantiated by the Apollo 11 solar-wind composition experiment (ref. 8–9). It was shown that solar-wind helium reaches the lunar surface in an unimpeded, highly directional flow.

[a] Physikalisches Institut, University of Bern.

[b] Institut für Kristallographie und Petrographie, Federal Institute of Technology, Zurich.

[†] Principal investigator.

Principle of the Experiment

An aluminum foil 30 cm wide and 140 cm long, with an area of approximately 4000 cm^2, was exposed to the solar wind at the lunar surface by the Apollo 12 crew on November 19, 1969, at 12:35 G.m.t. The foil was positioned perpendicular to the solar rays (fig. 8–1), exposed for 18 hr and 42 min, and brought back to Earth. Laboratory experiments (ref. 8–12) have determined that solar-wind particles, arriving with an energy of approximately 1 keV/nucleon, penetrate approximately 10^{-5} cm into the foil, and a large and calibrated fraction are firmly trapped. In the laboratory, the returned foil is analyzed for trapped solar-wind noble gas atoms. Parts of the foil are melted in ultra-high vacuum systems, and the noble gases of solar-wind origin thus released are analyzed with mass spectrometers for element abundance and isotopic composition. In addition, a search will be conducted for the possible presence in the solar wind of the radioactive isotopes tritium and ^{56}Co.

Instrumentation and Lunar Surface Operation

The experiment hardware was the same as that flown on Apollo 11 (ref. 8–8) and consisted of a metallic telescopic pole approximately 4 cm in diameter and approximately 40 cm in length when collapsed. In the stowed position, the foil was enclosed in the tubing and rolled up on a spring-driven roller. The instrument weighed 430 g. When extended at the lunar surface, the pole was approximately 1.5 m long and a 30- by 130-cm foil area was exposed. Only the foil assembly was recovered at the end of the lunar exposure period; it was rolled on the spring-driven roller and returned to Earth. Figure 8–1 shows the instrument as deployed on the lunar

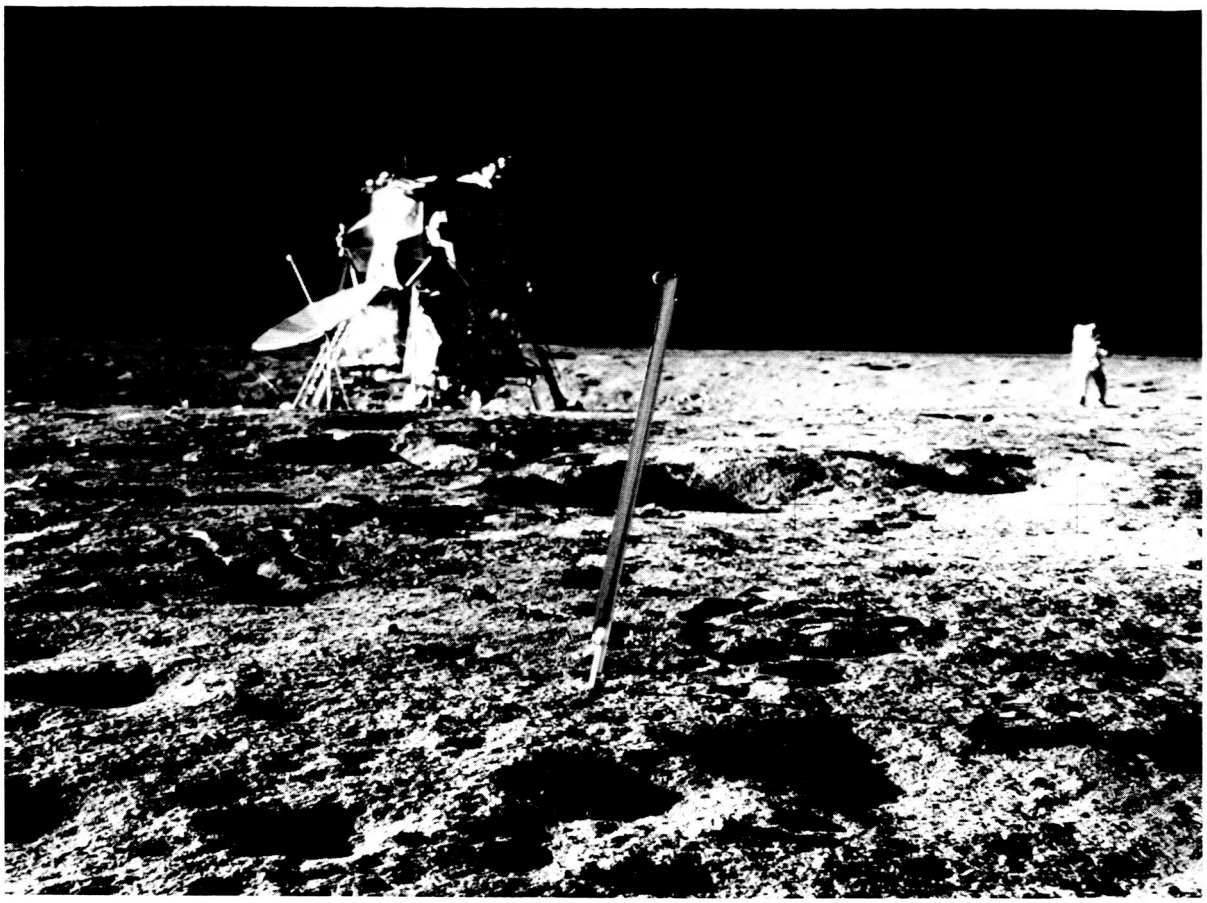

FIGURE 8-1. – Apollo 12 solar-wind composition experiment as deployed on the lunar surface (NASA photograph AS12-47-6899).

surface. By evaluating a number of Apollo 12 photographs, it was concluded that the foil was reclined by 10° during exposure. The average solar elevation during exposure was 13°, and thus the average direction of incidence of the sunlight on the foil was 3° above the foil normal.

After retrieval, the return unit was placed in a special Teflon bag and returned to Earth in the documented sample return container. In the Manned Spacecraft Center Lunar Receiving Laboratory (LRL), the unit was taken out of the Teflon bag, and the foil was inspected without unrolling it. The upper portion of the foil was found to be tightly and smoothly rolled. The outer windings of the foil were bulky. This, however, does not affect the quality of scientific data obtained from the experiment. Inside the Teflon return bag, a quantity of about a gram of fine lunar soil material was found, including grain sizes of 1 to 2 mm. This lunar material must have entered the bag during return or during postflight handling of the lunar sample return container. First analyses of light noble gases in the foil have shown that this dust contamination can be eliminated sufficiently by ultrasonic treatment. Dust contamination during return could be lowered by using a larger return bag, which can be closed more effectively.

Preliminary Results

The foil had the same dimensions, general makeup, and trapping properties as the Apollo 11 foil, described in detail in reference 8–8. Again, as on Apollo 11, test pieces were incorporated that had been irradiated before flight

with a calibrated amount of neon. In addition, an unirradiated test foil was mounted in a position that remained shielded from the solar wind.

In the Apollo 11 solar-wind composition experiment, part of the foil had been sterilized and released from the LRL before termination of the quarantine period for lunar material. No such early release was attempted with the Apollo 12 experiment foil to restrict foil handling and to avoid additional contamination with lunar dust in the LRL quarantine cabinets.

The Apollo 12 foil was received in the laboratory in the middle of January 1970. For the first analysis, three small foil pieces were decontaminated by means of the ultrasonic treatments that had proved their efficiency in the Apollo 11 foil analyses. The results of these first measurements are given in table 8–I. It may be seen that the shielded foil piece had a ^{4}He concentration per unit area that was less than 1 percent of the concentrations found in the foil pieces exposed to the solar wind. The agreement is good between the concentrations and the ^{4}He/^{3}He ratios measured in the two exposed foil pieces.

TABLE 8–I. *First Results From Apollo 12 Solar-Wind Composition Experiment Foil Analyses*

Sample number	*Elevation above lunar surface, cm*	*Area, cm^2*	*^{4}He concentration per unit area, $\times 10^{10}$ atoms/cm^2*	*^{4}He/^{3}He ratio*
Shielded foil:				
10-2	145	7.7	0.4	–
Exposed foil:				
10-1	139	9.8	45.6	2580
9-1	123	10.9	44.5	2610

The average ^{4}He flux during the Apollo 12 exposure period can be calculated by using the data given in table 8–I. The trapping probabilities of the foil for noble gas ions depend only slightly on energy in the general solar-wind velocity region. For helium with a velocity greater than 300 km/sec, the trapping probability is 89 ± 2 percent for normal incidence and 5 percent less for an incidence angle of 70° to 75°. In the Apollo 11 experiment, the angular distribution of the arriving helium ions has actually been determined (ref. 8–9). The same experiment with the Apollo 12 foil has not yet been completed; therefore, in this paper, the expected angle of incidence on the foil has been estimated. The average angle of incidence of the sunlight on the foil was 87°. The effects of corotation and aberration lower this value to about 84° for the solar wind (refs. 8–13 and 8–14). During the time of the Apollo 12 foil exposure, the Moon had probably already passed into the magnetosheath of the Earth, and the ion flow direction was changed relative to the undisturbed solar wind. The tilt of the magnetosphere (ref. 8–15) lowers the expected direction of incidence by approximately 5° (ref. 8–15), and an additional lowering by a few degrees can be expected as a result of the change of flow direction in the shockfront. Thus, the expected angle of incidence on the foil is 70° to 75°. With this assumption, the average ^{4}He flux during the Apollo 12 exposure period is as given in table 8–II and is compared with the flux observed during the Apollo 11 landing. The two figures are similar and are in good agreement with average fluxes derived from He/H ratios observed with solar-wind energy/charge spectrometers. (Compare with ref. 8–6.) The expected direction of solar-wind incidence is 25° to 30° above the lunar horizon. Even if helium would be heated to 1 to 2 million degrees centigrade in the shock transition, the portion of the helium flux cut off by the horizon would be negligible. Thus, the ^{4}He flux given herein should be directly comparable to fluxes obtained by Earth satellites during the same period.

TABLE 8–II. *Comparison Between the Preliminary Average ^{4}He Flux Obtained from the Apollo 12 Solar-Wind Composition Foil Exposure Period and the Flux Obtained From the Apollo 11 and the Flux Obtained From the Apollo 11 Solar-Wind Composition Experiment*

Mission	*Exposure initiated*	*Exposure duration*	*Average ^{4}HE flux, $\times 10^6$ atoms/cm^2-sec*
Apollo 11	July 21, 1969, 03:35 G.m.t.	77 min	6.3±1.2
Apollo 12	Nov. 19, 1969, 12:35 G.m.t.	18 hr 42 min	8.2±1.0

From the first two Apollo 12 foil pieces analyzed, ^{4}He/^{3}He $= 2600 \pm 200$ is obtained for the

Apollo 12 exposure period. This value is higher than the $^4He/^3He$ ratio obtained so far from the analyses of pieces of the Apollo 11 foil. Comparative analyses of pieces of foils from the two flights are being continued to confirm this difference. Actually, time variations in isotopic ratios in the solar wind can be expected (ref. 8–16), and the $^4He/^3He$ ratio has to be determined repeatedly to assess the range of occurring variations before an average for the present-day solar wind can be established. This average is of high astrophysical significance, since it can be compared with ancient $^4He/^3He$ ratios derived from solar-wind gases trapped in the lunar surface (ref. 8–17) or in meteorites. If a secular increase in the solar $^3He/^4He$ ratio should be found, this could be interpreted as a result of mixing inside the Sun or as a result of nuclear reactions at the solar surface.

The results obtained from the analyses of the first small pieces of the Apollo 12 foil indicate that, from larger foil areas, fluxes and isotopic composition can be obtained not only for helium but also for neon and argon.

Reference

8-1. Hundhausen, A. J.; Asbridge, J. R.; Bame, S. J.; Gilbert, H. E.; and Strong, I. B.: Vela-3 Satellite Observations of Solar Wind Ions: A Preliminary Report. J. Geophys. Res., vol. 72, no. 1, Jan. 1, 1967, pp. 87-100.

8-2. Snyder, C. W.; and Neugebauer, M.: Interplanetary Solar Wind Measurements by Mariner II. Space Research IV. Proceedings of the Fourth International Space Science Symposium, vol. IV, P. Muller, ed., North-Holland Pub. Co. (Amsterdam), 1964, pp. 89-113.

8-3. Wolfe, J. H.; Silva, R. W.; McKibbin, D. D.; and Mason, R. H.: The Compositional, Anisotropic, and Nonradial Flow Characteristics of the Solar Wind. J. Geophys. Res., vol. 71, no. 13, July 1, 1966, pp. 3329-3335.

8-4. Snyder, C. W.; and Neugebauer, M.: The Relation of Mariner-2 Plasma Data to Solar Phenomena. The Solar Wind, R. J. Mackin, Jr., and Marcia Neugebauer, eds., Pergamon Press, 1966, pp. 25-32.

8-5. Ogilvie, K. W.; Burlaga, L. F.; and Wilkerson, T. D.: Plasma Observations on Explorer 34. J. Geophys. Res., vol. 73, no. 21, Nov. 1, 1968, pp. 6809-6824.

8-6. Robbins, D. E.; Hundhausen, A. J.; and Bame, S. J.: Helium Abundance and Plasma Properties in the Solar Wind. Preprint ST531, Trans. Am. Geophys. Union, vol. 50, no. 4, April 1969, p. 302.

8-7. Bame, S. J.; Hundhausen, A. J.; Asbridge, J. R.; and Strong, I. B.: Solar Wind Ion Composition. Phys. Rev. Letters, vol. 20, no. 8, Feb. 19, 1968, pp. 393-395.

8-8. Geiss, J.; Eberhardt, P.; Signer, P.; Buehler, F.; and Meister, J.: The Solar-Wind Composition Experiment. Apollo 11 Preliminary Science Report, sec. 8, NASA SP-214, 1969, pp. 183-186.

8-9. Buehler, F.; Eberhardt, P.; Geiss, J.; Meister, J.; and Signer, P.: Apollo 11 Solar Wind Composition Experiment: First Results. Science, vol. 166, no. 3912, Dec. 19, 1969, pp. 1502-1503.

8-10. Lyon, E. F.; Bridge, H. S.; and Binsack, J. H.: Explorer 35 Plasma Measurements in the Vicinity of the Moon. J. Geophys. Res., vol. 72, no. 23, Dec. 1, 1967, pp. 6113-6117.

8-11. Ness, N. F.; Behannon, K. W.; Scearce, C. S.; and Cantarano, S. C.: Early Results from the Magnetic Field Experiment on Lunar Explorer 35. J. Geophys. Res., vol. 72, no. 23, Dec. 1, 1967, pp. 5769-5778.

8-12. Buehler, F.; Geiss, J.; Meister, J.; Eberhardt, P.; Huneke, J. C.; and Signer, P.: Trapping of the Solar Wind in Solids, Part 1. Trapping Probability of Low Energy He, Ne, and Ar Ions. Earth and Planet. Sci. Letters, vol. 1, no. 5, Sept. 1966, pp. 249-255.

8-13. Hundhausen, A. J.: Direct Observations of Solar-Wind Particles. Space Sci. Rev., vol. 8, no. 4, Sept. 24, 1968, pp. 690-749.

8-14. Axford, W. I.: Observations of the Interplanetary Plasma. Space Sci. Rev., vol. 8, no. 3, Jan. 5, 1968, pp. 331-365.

8-15. Hundhausen, A. J.; Bame, S. J.; and Asbridge, J. R.: Plasma Flow Pattern in the Earth's Magnetosheath. J. Geophys. Res., vol. 74, no. 11, June 1, 1969, pp. 2799-2806.

8-16. Geiss, J.; Hirt, P.; and Leutwyler, H.: On Acceleration and Motion of Ions in Corona and Solar Wind. Solar Physics, 1970 (in press).

8-17. Proceedings of the Lunar Science Conference. Science, vol. 167, no. 3918, Jan. 30, 1970, pp. 449-784.

9. Apollo 12 Multispectral Photography Experiment

A. F. H. Goetz,[a†] *F. C. Billingsley,*[b] *E. Yost,*[c] *and T. B. McCord* [d]

The lunar multispectral photography experiment was successfully accomplished on Apollo 12. A number of photographs were returned in the blue, green, red, and infrared (IR) portions of the optical spectrum. Preliminary data analysis shows no color boundaries in the frame containing the Fra Mauro formation and the Apollo 13 landing site. Color differences were found in the frame containing Lalande η, establishing the existence of small-scale color differences on the lunar surface.

Purpose of the Experiment

The goal of the lunar multispectral photography experiment was to obtain vertical strip photography in three portions of the optical spectrum – blue, red, and IR – at resolution one to two orders of magnitude higher than is obtainable from Earth. A fourth camera, which had a green filter, was added to the array for operational purposes. However, for the sake of the following discussion, this camera will be considered to be part of the experiment.

The further objectives of this experiment were as follows:

(1) To photograph future Apollo landing sites so that ground-truth information provided by the returned samples may be extrapolated to other points on the lunar surface

(2) To produce photometrically accurate, two- and three-color images by photographic and computer processing methods that will accurately delineate lunar color boundaries and their magnitudes

(3) To evaluate, under closely controlled conditions, the photographic versus the computer image-processing techniques for reduction of lunar multispectral photography

Lunar Color Measurement

Lunar color and its variation across the lunar surface have interested planetary astronomers for many years. The interest has heightened with the growing weight of evidence, obtained from accurate Earth-based photoelectric photometry, that points toward a positive correlation between color and compositional differences (ref. 9–1). Once ground-truth samples have been obtained at several sites of differing color, it may be possible to extrapolate compositional color information to large areas of the Moon that will not be sampled *in situ*.

In the present context, color differences mean relative differences in spectral reflectivity between points on the surface. The general spectral reflectivity curve of the Moon shows a near-linear increase in reflectivity from 400 to 800 nm (ref. 9–2). Areas designated red or blue reflect more energy in their respective wavelength regions than a standard lunar area. In most cases, the greater the separation in wavelength, the greater the color difference obtained. The differences between 400 and 800 nm, among points on the lunar surface, average 4–8 percent (ref. 9–1).

Photographic (ref. 9–3) and photoelectric (ref. 9–1) methods have been used in the past for the measurement of lunar color variations. The best known photographic method used to date is Whitaker's sandwich printing technique (ref. 9–3) in which a negative ultraviolet plate and a positive IR plate are sandwiched together and printed. Color differences then show up as varying shades of gray. The disadvantages of

[a] Bellcomm, Inc., Washington, D.C.
[b] JPL, California Institute of Technology.
[c] Long Island University.
[d] Massachusetts Institute of Technology.
[†] Principal investigator.

this method are that it is not quantitative and that albedo changes can masquerade as color differences if the density-logarithm-exposure (D log E) curves of the two plates are not extremely well matched. The advantage of the method lies in the image form of data display.

Recent advances in photoelectric instrumentation allow ground-based relative color measurements to be made to 0.1 percent accuracy (ref. 9–4). Spectral reflectivity measurements of the Apollo 11 soil samples show an excellent correlation with ground-based telescope data of the Tranquility site (ref. 9–5). However, point-by-point measurement is a time-consuming process and is not suited for image display. Work now in progress with electronic imaging systems incorporates the advantages of both methods.

Computer image processing (ref. 9–5) of photographs combines the advantages of photographic image display and provides quantitative color information for the entire picture, although at accuracies less than are obtainable from photoelectric photometry.

Equipment and Operation

The experiment camera array consisted of four 70-mm Hasselblad cameras with 80-mm lenses. The filter and black-and-white film combinations were as follows: blue 47B filter, type 3401 film; green 58 filter, type 3401 film; red 29 + 0.6ND filter, type 3401 film; and infrared 87C filter, type SO-246 film. Type 3401 is Plus-X aerial film, and type SO-246 is type 5424 infrared aerographic film coated on a 4-mil base. The center wavelength of each filter/film combination is as follows: blue, 430 nm; green, 540 nm; red, 660 nm; and IR, 860 nm.

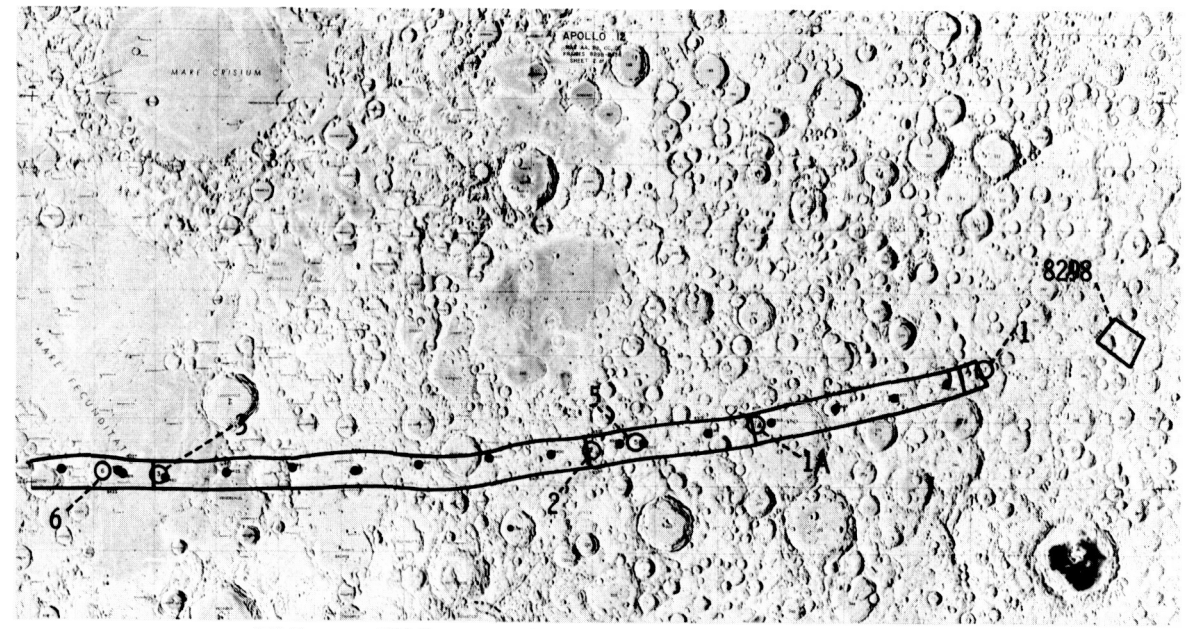

Legend

1. Start blue, green, red stereo sequence (1/60, f/5.6)
1A. Start IR (1/60, f/4.0)
2. All stop
3. Start blue, green, red
5. All start (blue, green, IR, f/8.0) second revolution (red, f/5.6)
6. All stop
• Principal point

FIGURE 9-1. — Apollo 12 multispectral photography ground track from 135° E to 45° E.

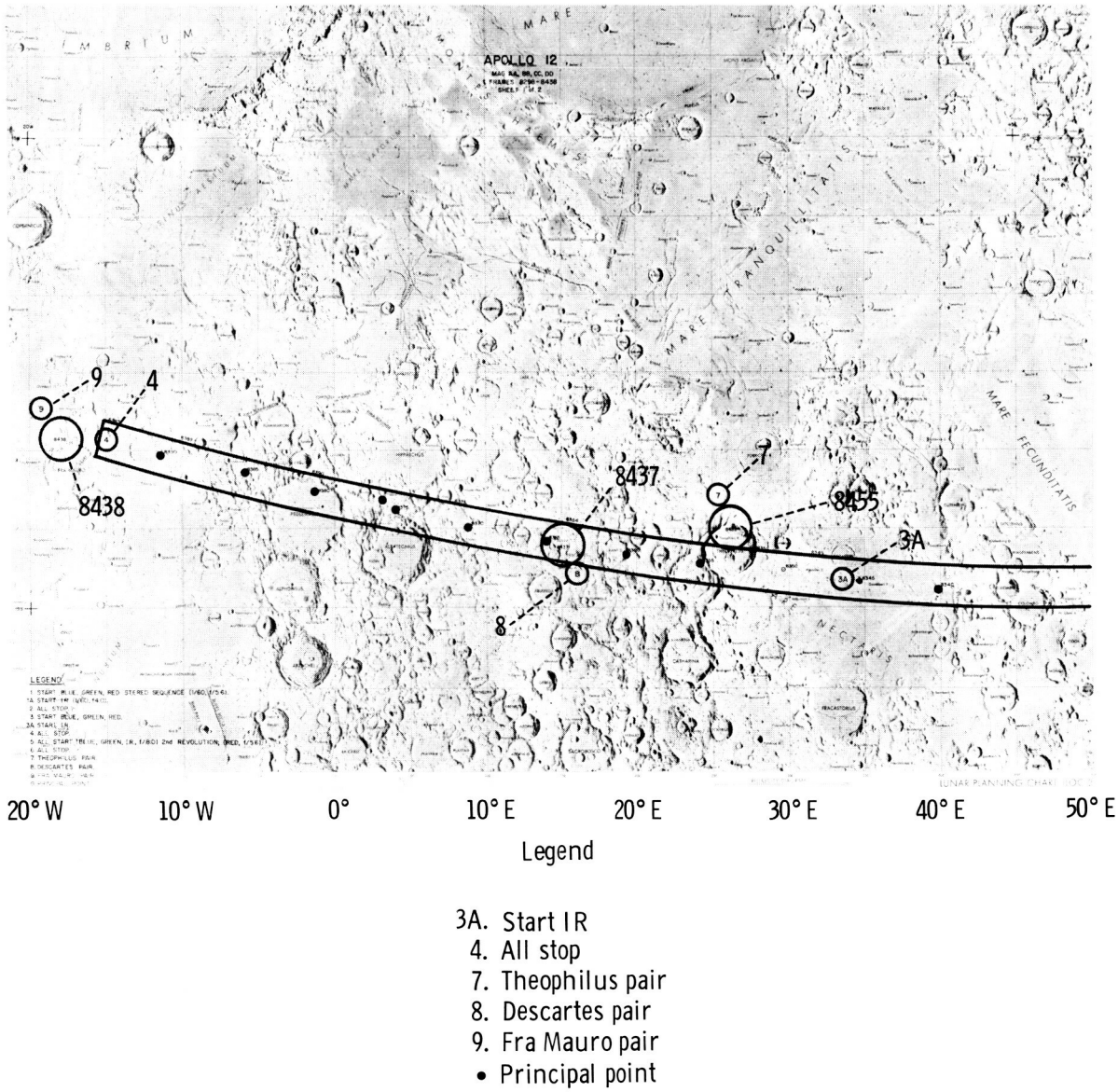

FIGURE 9-2. — Apollo 12 multispectral photography ground track from 50° E to 20° W.

An intervalometer tripped all shutters simultaneously at 20-sec intervals. For operational purposes, the shutter speed on all four cameras was fixed at 1/60 sec. Focus settings were fixed at 44 ft for the IR camera and at infinity for the other three cameras. To facilitate *f*-stop changes, the vertical strip photography was broken into three segments. During orbital revolution 27, the blue, green, and IR cameras were set at *f*/5.6, and the red camera was set at *f*/4.0. Photography was taken between longitudes 120° E and 90° E and between 54° E and 15° W. The minimum Sun angle was approximately 25°. The remainder of the vertical photography was carried out on revolution 28 at *f*/8/5.6. The off-vertical targets of opportunity were exposed at *f*/5.6/4.0 for Theophilus and Descartes and at *f*/2.8/2.8 for Fra Mauro. Figures 9–1 and 9–2 show the photography ground track.

Film Calibration and Processing

All flight-film calibration and processing were accomplished by the NASA Manned Spacecraft Center (MSC) Photographic Technology Laboratory (PTL). Preflight calibration was accomplished by applying a 21-step gray wedge to the film in a 1-B sensitometer. For the experiment, a special step tablet was constructed to provide four 21-step wedges arranged to fit in a 60- by 60-mm format to facilitate film-scanning procedures. In addition, a preflight standard wedge and a postflight special tablet were applied to the leader of the film.

Preflight process controls were established to develop the films to the following gammas: blue, 1.7; green, 1.65; red, 1.6; and IR, 1.5. The different gammas were chosen to compensate for the increasing transmission of the standard wedge toward longer wavelengths. In other words, the absolute gamma should be 1.7 for each film. The relatively high gammas were chosen to give the maximum exposure differentiation commensurate with the required dynamic range on the film. The following gammas were obtained: blue, 1.68; green, 1.48; red, 1.42; and IR, 1.44. The reasons for the discrepancy among control and flight-film gammas are not completely understood but can probably be attributed to radiation fogging and latent image decay. The PTL is investigating this effect.

Film Return

Each of the blue-, green-, and red-filtered cameras returned 142 frames, while the IR camera, in which the film had been rationed, returned 105 frames. The resolution in the returned type 3401 film is approximately 30 m. This limit is approximately the motion resulting from the shutter speed of 1/60 sec. The densities on all frames fell within the approximate straight-line portion of the respective D log E curves shown in figure 9–3. This requirement was necessary for data reduction by photographic methods. For reasons not understood at this time, all IR frames have a 4-mm-wide underexposed strip at the leading and trailing edges of each frame. The IR frames are not in focus because of an apparent film-magazine malfunction, and they will not be usable for color difference analysis.

Data Reduction

The color or spectral reflectivity differences sought in this study are not detectable by eye or on normal color film. The eye is very sensitive to small color variations under controlled laboratory conditions, in particular when the objects have the same brightness and are juxtaposed. However, the eye is incapable of reliably detecting small differences in spectral reflectivity in conjunction with brightness differences such as in a lunar surface scene. Normal color-additive techniques using color-separation photographs also fail to show up differences, even at higher saturation.

The two methods mentioned previously – the photographic sandwich and computer image processing techniques – are basically techniques for ratioing two pictures. Ratioing is necessary to remove the brightness variations caused by general albedo and slope differences. Because the film density is a function of the logarithm of the exposure, ratios are formed by taking differences in densities between two pictures. Such difference pictures for two colors have been produced by photographic (ref. 9–3) and computer (ref. 9–6) methods. Data reduction for the experiment will be carried out in three colors by using extensions of both methods. Details of these procedures will be the subject of later publications.

Photographic data reduction to date has included construction of three-color difference pictures of five frame sets. The main difficulties in analyzing these composites are anomalous colors introduced by nonlinearities in the D log E curves (which limit the range of brightnesses for which the color construction is valid) and brightness nonuniformities that are due to camera vignetting. While several frames show color differences, more work must be completed on establishing confidence limits before interpretations can be made.

Extensive computer image processing has been accomplished on only two frames: 8438 and 8392. Only two-color difference pictures have been constructed to date by methods used previously on Earth-based photography (ref. 9–6). The basic method consists of the following steps:

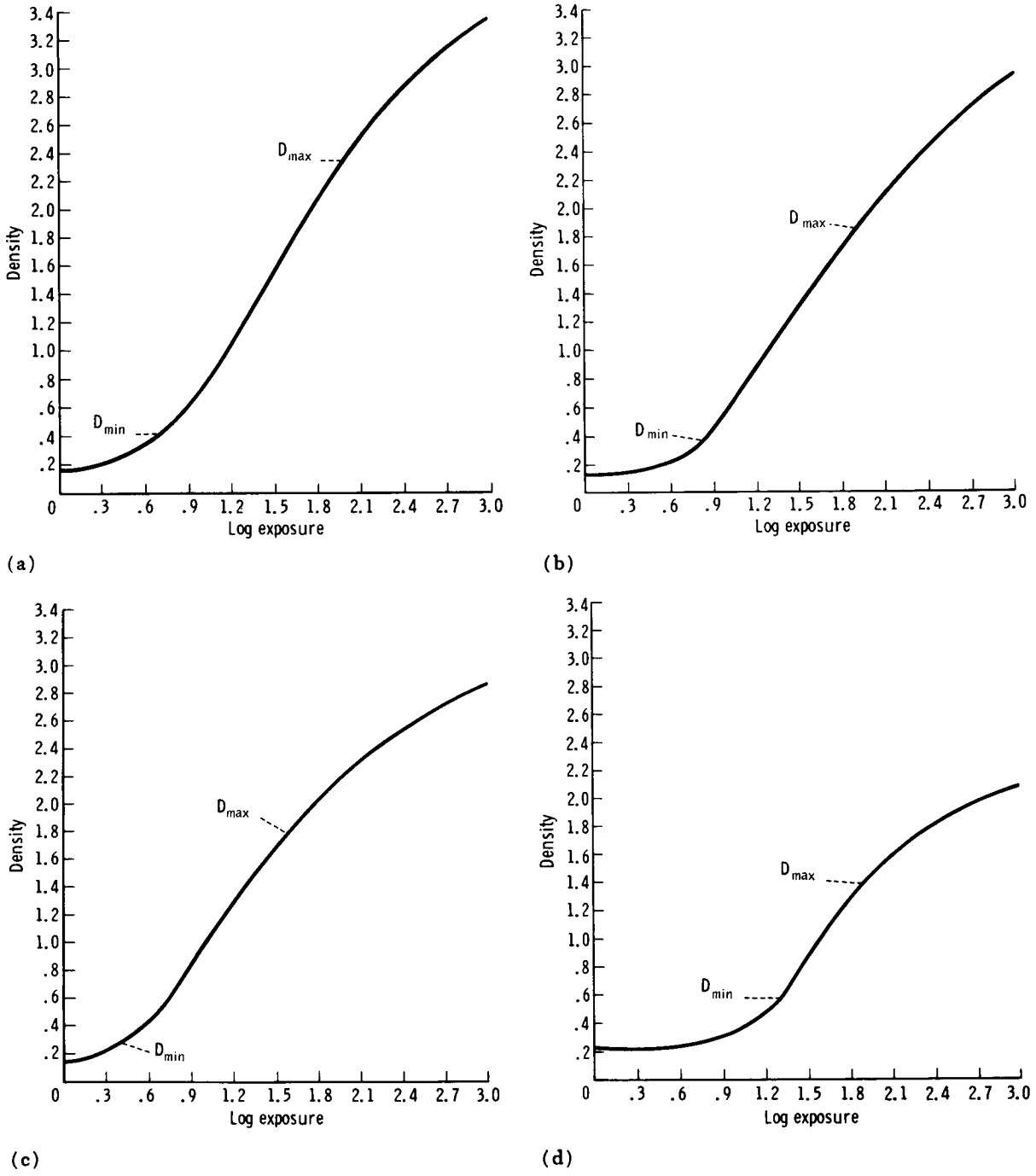

FIGURE 9-3. – Processing curves obtained from preexposed standard wedge. (a) Blue filter. (b) Green filter. (c) Red filter. (d) Infrared.

(1) Scanning by video film converter (VFC) of each set of pictures, including the preflight calibration step tablets (scanning spot sizes of 25, 40, and 50 μm have been used)

(2) Obtaining a VFC response curve and linearizing the D log E curve

(3) Converting all points (1 to 2×10^6 points per frame) to the log E domain, thus eliminating

any film sensitivity or processing differences between colors

(4) Registration of the frames of the two colors to be differenced

(5) Point-by-point subtraction and normalization of two frames

(6) Contrast stretching, up to a factor of 3, so that each step in log E becomes visible as a distinct shade of gray (the step size is approximately 2.5 percent in exposure)

(7) Replaying the picture onto film

The registration of the frames has been the major problem encountered. Each camera/filter combination exhibits different geometrical distortions and a slightly different magnification. These systematic distortions are coupled with near-random distortions that are due to lack of film flatness. Good registration can be facilitated only by brute-force rubber-sheet stretching programs.

Figure 9–4 shows frame 8438, a view of the Fra Mauro formation and the Apollo 13 landing site, taken with the blue-, green-, and red-filtered cameras. The dark corner in each picture is the result of obscuration by the edge of the hatch window. No noticeable density variations, other than an overall brightness difference, are visible. Two-color computer difference pictures, blue minus green and red minus blue, have been produced. The composites show no significant color differences over the entire frame, including the mare-highlands boundary. Some implications of this result are given in the following paragraphs.

A two-color difference picture of frame 8392

(a)

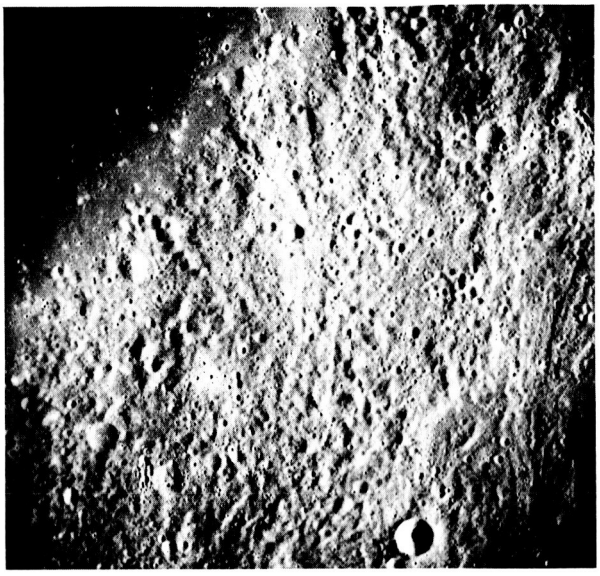

(b)

(c)

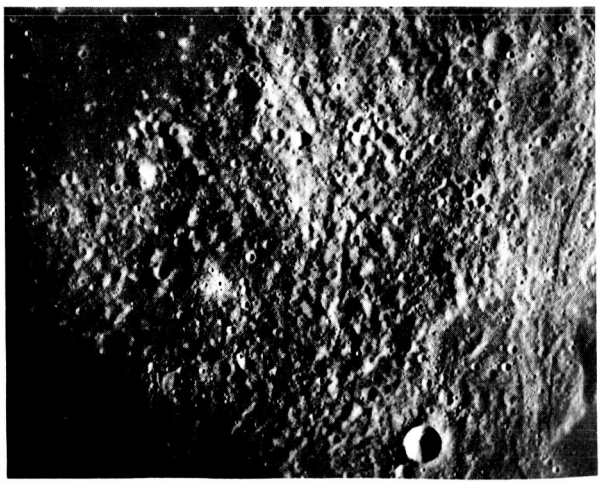

FIGURE 9-4. – Fra Mauro formation and Apollo 13 landing site. (North is at the top of the photos.) (a) Blue filter (AS12-56B-8438). (b) Green filter (AS12-56D-8438). (c) Red filter (AS12-56C-8438).

(fig. 9–5), which covers a portion of Mare Nubium and Lalande η, was constructed. Figure 9–6 is a contrast-stretched red-minus-blue print of frame 8392 in which dark areas are bluer and light areas are redder than an arbitrary point that was chosen to be gray.

Distinct color differences are evident, in particular between Lalande η and the surrounding mare and between what appears to be secondary-impact ejecta rays and the surrounding mare. Although the frames have not been calibrated for camera vignetting or adjusted to a lunar standard by Earth-based photometry, there is now, for the first time, clear evidence for local small-scale color variations on the lunar surface.

FIGURE 9-5. – Two-color difference picture of frame 8392 covering a portion of Mare Nubium and Lalande η.

Discussion

Differences in spectral reflectivity can be caused by several factors. Compositional variations give rise to color differences. However, subtle differences, such as recorded in frame 8392, may very well be caused by variations in the iron and titanium content of the glasses, as in the Apollo 11 sample described by Adams and Jones (ref. 9–5).

Particle size affects the slope of the reflectivity curve of rock materials. Typically, for basaltic materials in the laboratory, the sample becomes redder with decreasing particle size (ref. 9–7).

The effects of age on color appear to be insignificant, at least with respect to alteration of the optical properties of *in situ* materials by the lunar environment. No evidence for metal coatings or deposits of sufficient thickness to affect the optical properties was found on mineral grains in the Apollo 11 sample (ref. 9–5). On the basis of telescopic measurements, McCord (ref. 9–1) finds no evidence of an aging effect that causes color variations.

Frame 8392, which contains Lalande η, exhibits definite color differences, as shown in figure 9–6. Careful inspection reveals that color is not directly correlated with brightness, particularly as seen in the comparison of the boundary between the embayment and the mare on the east side of Lalande η and the boundary on the flat southeastern side of the same feature. Therefore, except in the deep shadows, the color variations are real and are not artifacts produced by photographic nonlinearities.

The white streaks in the mare appear to be impact ejecta plumes, probably produced by secondaries from the crater Lalande η. It is not apparent whether the light material is secondary projectile material or material that has been excavated from beneath the mare surface. The plumes are bluer than the surrounding mare, and their boundaries are sharp on a 100-m scale. The color difference runs contrary to the observation that in basaltic rocks, finer higher-albedo material is redder. Therefore, a compositional difference must be assumed to explain the bluer plumes.

If, indeed, the plume material has been excavated from below the mare surface, then the material must have been ejected from craters smaller than about 30 m in size, since no single plume-source crater is visible and since the smaller craters are below the resolution limit of the film. For such a case, the thickness of the dark surface material is limited to 7 to 10 m. On a small scale, the blue, bright plumes are similar to the feature Reiner γ, which exhibits a similar color difference.

The absence of color variations in frame 8438, particularly at the mare boundary, is somewhat

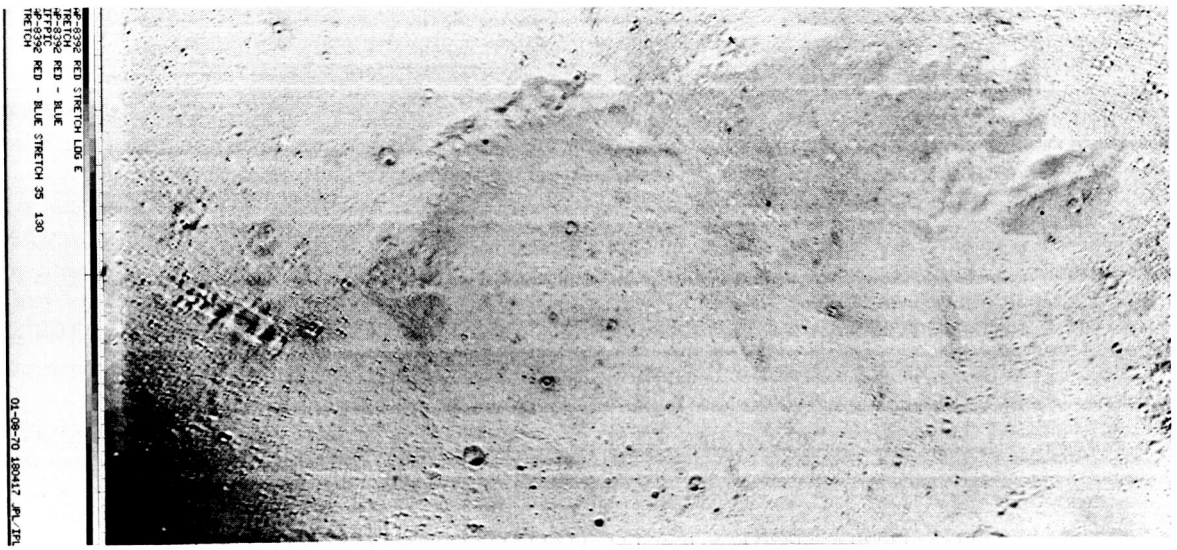

FIGURE 9-6. — Contrast-stretched red-minus-blue difference picture of the center portion of frame 8392. Dark areas are bluer and light areas are redder than an arbitrary point taken as neutral gray. The light vertical banding is an artifact introduced in the scanning process. Slight misregistration of the red and blue frames enhances crater boundaries. In addition, color information cannot be obtained from deep shadow areas; hence, those areas will appear anomalously colored.

surprising but not without precedent. McCord (ref. 9–1) has found a similar lack of contrast across some mare-upland boundaries between average areas 18 km in diameter. Since a definite albedo and morphological discontinuity are present, a color boundary would be expected. A mean particle-size difference has been suggested as the cause of the mare-upland albedo differences observed (ref. 9–8). However, such a size difference would be expected to result in a color difference. The analysis of the Apollo 13 samples should solve this dilemma. Furthermore, more detailed reduction and analysis of multispectral photographs will better define the power of this method in the interpretation of lunar surface geology.

Summary

The lunar multispectral photography experiment has yielded 142 black-and-white photographs, taken with blue-, green-, red-, and IR-filtered cameras, that are suitable for color-difference analysis. Two existing image data-reduction methods are being expanded to produce images that display greatly enhanced three-color contrast. Two-color difference pictures have been produced, and the method has been shown to be effective. The color enhancement of the Apollo 13 landing-site frame shows a somewhat surprising lack of color variation. The frame containing Lalande η exhibits color differences, the first such differences to be detected in high-resolution photography of the lunar surface, which probably can be attributed to compositional variations.

References

9-1. McCORD, T. B.: Color Differences on the Lunar Surface. J. Geophys. Res., vol. 74, no. 12, June 15, 1969, pp. 3131-3142.

9-2. McCORD, T. B.: Color Differences on the Lunar Surface. Ph. D. Dissertation, Calif. Inst. of Tech., 1968.

9-3. HEACOCK, R. L.; KUIPER, G. P.; SHOEMAKER, E. M.; UREY, H. C.; and WHITAKER, E. A.: Ranger VII, Part II: Experimenters' Analyses and Interpretations. TR 32-700, JPL, Calif. Inst. of Tech., Feb. 1965.

9-4. McCORD, T. B.: A Double-Beam Astronomical Photometer. Applied Optics, vol. 7, no. 3, Mar. 1968, pp. 475-478.

9-5. ADAMS, J. B.; and JONES, R. L.: Spectral Reflectivity of Lunar Samples. Science, vol. 167, no. 3918, Jan. 30, 1970, pp. 737-739.

9-6. BILLINGSLEY, F. C.; GOETZ, A. F. H.; and LINDSLEY, J. N.: Color Differentiation by Computer Image Processing. Photographic Science and Engineering, vol. 14, no. 1, Jan. 1970, pp. 28-35.

9-7. ADAMS, J. B.; and FILICE, A. L.: Spectral Reflectance 0.4 to 2.0 Microns of Silicate Rock Powders. J. Geophys. Res., vol. 72, no. 22, Nov. 15, 1967, pp. 5705-5715.

9-8. ADAMS, J. B.: Lunar Surface Composition and Particle Size: Implications from Laboratory and Lunar Spectral Reflectance Data. J. Geophys. Res., vol. 72, no. 22, Nov. 15, 1967, pp. 5717-5720.

ACKNOWLEDGMENTS

The authors wish to thank Jurrie van der Woude of the California Institute of Technology for his invaluable assistance in obtaining telescope test photography. Richard R. Baldwin of MSC made an outstanding effort in coordinating the hardware and flight plan integration. Noel T. Lamar of MSC was instrumental in expediting the stringent film processing requirements.